Coherent atomic waveguides from hollow optical fibers: quantized atomic motion

S. Marksteiner, C. M. Savage,* and P. Zoller

Joint Institute for Laboratory Astrophysics, University of Colorado, Boulder, Colorado 80309

S. L. Rolston

National Institute of Standards and Technology, Gaithersburg, Maryland 20899

We present a theoretical analysis of coherent atomic motion through a straight atomic waveguide constructed from a hollow optical fiber. Atoms are guided by the evanescent light field at the fiber's interior glass-vacuum interface. The atoms' internal structure is modeled by a $J_g=0$ to $J_e=1$ transition. The atomic wave functions are determined and the loss rates due to spontaneous emission, tunneling to the wall, and nonadiabatic transitions are estimated. The influence of Casimir-Polder forces is considered. We conclude with a discussion of the feasibility of the proposed waveguides.

PACS number(s): 42.50.Vk, 42.81.Qb

I. INTRODUCTION

Light tuned above resonance exerts a mechanical force repelling atoms from regions of high light intensity. This is due to the electric dipole interaction between the light and atom [1–4]. In the laboratory this force has been used to reflect atoms from evanescent light fields on the surface of glass [5–9]. Evanescent light fields have strong intensity gradients and hence can exert strong repulsive forces on atoms. In this paper we consider how the evanescent field on the interior of a hollow optical fiber can be used to guide atoms through the fiber [10].

Such a waveguide is analogous to a cylindrical hollow microwave waveguide. The wave equation and conducting boundary conditions determine the modes of a microwave waveguide. For an atomic waveguide the Schrödinger equation and repulsive evanescent field determine the modes. The decay length of the evanescent field is approximately the wave number of the light, about 0.1 μm for visible light. Hence the evanescent field approximates a step potential, forcing the confined atomic wave functions toward zero at the fiber's wall.

The evanescent light field is found by a standard dielectric waveguide analysis of the hollow optical fiber. In order to get large evanescent fields the light propagating in the glass fiber must be confined to as small a transverse area as possible. Hence we consider fibers that are optically single mode, having hole and core dimensions of a few micrometers. Even so, the maximum confined transverse atomic velocities are only a few centimeters per second, corresponding to cooled atoms.

The atomic dynamics is governed by the Schrödinger equation with an electric dipole coupling to the evanes-

cent field. The relevant atomic transition is assumed to be $J_g=0$ to $J_e=1$. We consider a straight fiber so that the motion along the fiber is decoupled from that in the confined transverse directions. We have not considered the effect of bends in the fiber. A WKB approximation is used to calculate the transverse eigenfunctions, from which the loss rates are then estimated [11]. We are concerned with preserving the quantum-mechanical coherence of the atoms during the propagation. This is a requirement if the guided atoms are to be used for interferometry. We assume that spontaneous emission causes atoms to be lost from such coherent propagation. This is the major loss mechanism except for highly excited wave functions for which tunneling to the wall dominates.

An alternative type of hollow atomic waveguide has been proposed by Ol'Shanii *et al.* [12]. Their approach uses a conducting type optical waveguide and therefore has light propagating down the hollow region which also guides the atoms. The light is tuned *below* atomic resonance so that the atoms are attracted to the intensity maximum in the hole's center and away from the walls. An advantage of our scheme is that the atoms only interact with the light in a thin region near the walls instead of throughout the guidance region. This minimizes spontaneous emission, which is essential for ensuring coherent transport.

This paper is organized as follows. In Sec. II the optical properties of a hollow optical fiber are calculated and described. This gives us specific evanescent fields on which to base our subsequent analysis of the atomic guidance. Section III introduces the Schrödinger equation and constructs WKB approximations to the atomic transverse wave functions. In Sec. IV estimates of the loss rates from these wave functions are made. Losses are due to spontaneous emission, tunneling to the fiber's wall, and nonadiabatic transitions to attracting, instead of repelling, adiabatic potentials. The effect of the Casimir-Polder force is also estimated. Finally in Sec. V our results are related to realistic systems for guiding sodium or cesium atoms.

---

*Permanent address: Department of Physics and Theoretical Physics, Faculty of Science, Australian National University, Australian Capital Territory 0200, Australia.

<u>50</u>	2680

II. ELECTROMAGNETIC FIELDS IN HOLLOW FIBERS

In this section we investigate the modal structure of a hollow optical fiber. The fiber is modeled by a piecewise constant, cylindrically symmetric refractive index profile $n(x, y, z) = n(r)$, where $r = \sqrt{x^2 + y^2}$ is the distance from the symmetry axis and

$$n(r) = \begin{cases} 1 & \text{for } r < \rho_1 & \text{(I)} \\ n_F & \text{for } \rho_1 \leq r < \rho_2 & \text{(II)} \\ n_{Cl} & \text{for } r \geq \rho_2 & \text{(III)}. \end{cases} \quad (1)$$

Here ρ_1 is the radius of the hole and ρ_2 is the radius of the interface between the annular core and the cladding, which is assumed to extend to infinity. The magnetic permeability of the glass is assumed to be equal to the vacuum permeability μ_0. To calculate the electromagnetic field modes which represent unattenuated propagation along the fiber, we follow the procedure of Ref. [13]. These modes can be written in the form

$$\boldsymbol{E}(x, y, z) = \boldsymbol{e}(x, y)e^{i(\beta z - \omega t)} + \text{c.c.},$$

$$\boldsymbol{H}(x, y, z) = \boldsymbol{h}(x, y)e^{i(\beta z - \omega t)} + \text{c.c.}, \quad (2)$$

where $\boldsymbol{E}$ is the electric field, $\boldsymbol{H}$ is the magnetic field, β is the propagation constant along the fiber, and $\omega = ck$ is the angular frequency of the incident field. It is shown in Ref. [13] that the z components of the field amplitudes $\boldsymbol{e} = \boldsymbol{e}_t + e_z \hat{\boldsymbol{z}}$ and $\boldsymbol{h} = \boldsymbol{h}_t + h_z \hat{\boldsymbol{z}}$ obey Helmholtz equations

$$(\nabla_t^2 + n^2 k^2 - \beta)e_z = 0, \quad (\nabla_t^2 + n^2 k^2 - \beta)h_z = 0, \quad (3)$$

within each region of constant refractive index n. Here $\nabla_t = \hat{\boldsymbol{x}}\frac{\partial}{\partial x} + \hat{\boldsymbol{y}}\frac{\partial}{\partial y}$ denotes the transverse gradient operator. The transverse components $\boldsymbol{e}_t$ and $\boldsymbol{h}_t$ are related to e_z and h_z according to [Ref. [13], Eqs. (11)–(43)]

$$\boldsymbol{e}_t = \frac{i}{p}\left\{\beta\nabla_t e_z - \sqrt{\frac{\mu_0}{\varepsilon_0}}k\hat{\boldsymbol{z}} \times \nabla_t h_z\right\},$$

$$\quad (4)$$

$$\boldsymbol{h}_t = \frac{i}{p}\left\{\beta\nabla_t h_z + \sqrt{\frac{\varepsilon_0}{\mu_0}}kn^2\hat{\boldsymbol{z}} \times \nabla_t h_z\right\},$$

where $p = n^2 k^2 - \beta^2$ and ε_0 is the vacuum dielectric constant.

Thus we are left with the problem of solving the Helmholtz equation (3) in each of the regions (I)–(III). These solutions have to be matched at the boundaries, so that the magnetic field $\boldsymbol{H}$, the tangential component of the electric field $\boldsymbol{E}_{\|}$, and the normal component of the dielectric displacement vector $\varepsilon_0 n^2 \boldsymbol{E}_{\perp}$ are continuous. The solutions of the Helmholtz equation (3) are separable in polar coordinates and have the form

$$e_z(r, \phi) = \begin{cases} c_1 I_\nu(Ur/\rho_1)e^{i\nu\phi} & \text{(I)} \\ [c_2 J_\nu(Xr/\rho_1) + c_3 Y_\nu(Xr/\rho_1)]\,e^{i\nu\phi} & \text{(II)} \\ c_4 K_\nu(Wr/\rho_1)e^{i\nu\phi} & \text{(III)}, \end{cases}$$

$$\quad (5)$$

where

$$U = \rho_1\sqrt{\beta^2 - k^2}, \quad (6a)$$

$$X = \rho_1\sqrt{n_F^2 k^2 - \beta^2}, \quad (6b)$$

$$W = \rho_1\sqrt{\beta^2 - n_{Cl}^2 k^2}, \quad (6c)$$

and I_ν, K_ν, J_ν, and Y_ν are Bessel functions of integer order $\nu = 0, \pm 1, \pm 2, \ldots$ and $c_1, \ldots, c_4$ are unknown constants.

The solution for h_z is identical to Eq. (5) with the substitutions $e_z \rightarrow h_z$ and four additional constants $c_n \rightarrow c_{n+4}$. Matching these solutions at the hole-core interface ρ_1 and at the core-cladding interface ρ_2 leads to eight linear, homogeneous equations for these eight unknowns. These equations are listed in the Appendix. The nontrivial solutions determine the electromagnetic eigenmodes of the hollow fiber and in particular their propagation constant β as a function of ω and the fiber parameters.

For the guidance of atoms along the fiber it is desirable that the electric field does not have a static zero anywhere on the wall. In this case there would be no evanescent field to repel the atoms. The electric field inside the fiber is in general very complex since it is a superposition of all allowed eigenmodes. The amplitudes and phases of the various modes depend strongly on the way the incident laser light is coupled into the fiber. Another factor that might complicate the description of the fields is the coherence length of the laser light. This determines whether the superposition is a coherent or incoherent one. To circumvent these difficulties, we choose to concentrate on single-mode fibers, even though most of our conclusions are valid for multimode fibers.

To investigate the structure of the evanescent wave inside the hole, we first calculate the dependence of the propagation constants β_ν of the various modes on the hole radius ρ_1, while keeping the core thickness $\Delta\rho = \rho_2 - \rho_1$ constant. A plot of the modes $\nu = 0, 1, 2$ is shown in Fig. 1. The independent parameters in this problem
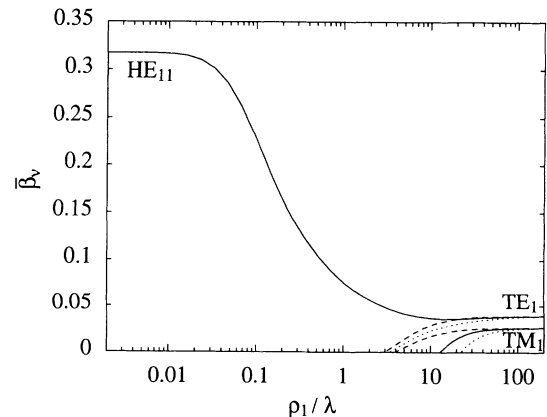

FIG. 1. Modal structure: normalized propagation constant $\bar{\beta}_\nu$ for $\nu=0$ (dashed), $\nu=1$ (solid), and $\nu=2$ (dotted) vs hole radius for the fiber parameters of Table I.

are $\rho_{1,2}/\lambda$, β/k, and $n_{F,Cl}$, and therefore we plot a normalized propagation constant $\bar{\beta}_\nu$, defined by

$$\bar{\beta}_\nu = \frac{\beta_\nu/k - n_{Cl}}{n_F - n_{Cl}}, \tag{7}$$

as a function of ρ_1/λ. It is easy to check that $0 \le \bar{\beta}_\nu \le 1$ and that $\bar{\beta}_\nu = 0$ corresponds to the cutoff of the νth mode (if it exists at all). For a hole radius going to infinity, the modal structure is very similar to that of an asymmetric planar waveguide [13]. In this limit we find highly degenerate values for the propagation constants, which correspond to TE and TM modes of the slab waveguide.

This degeneracy is removed for finite values of the hole radius. Decreasing the hole radius ρ_1 (while keeping the core thickness $\triangle\rho$ constant) leads to the disappearance of modes as they get cut off. Under certain conditions, all modes except the fundamental mode HE_{11} are cut off at a critical hole radius ρ_{1c} [14]. In Fig. 2, the region below the solid line shows the parameter regime where the hollow fiber is single mode for the refractive indices given in Table I. The dashed line corresponds to the cutoff for the TE_1 modes of the slab waveguide. For a core thickness close to this cutoff we can have, in principle, an arbitrarily large hole radius. Strictly, the HE_{11} mode represents two degenerate modes, corresponding to two linearly independent polarizations. By using appropriately polarized laser light to illuminate the fiber, we can ensure that only one of the two modes is excited.

As a specific case for later calculations we use the fiber parameters in Table I. We chose the refractive indices of the core and the cladding to be $n_F = 1.500$ and $n_{Cl} = 1.497$, respectively. A core thickness and a hole radius of $\triangle\rho = \rho_1 = 2.889\lambda$ (corresponding to 1.65 μm for the sodium D line) ensures that this hollow fiber is single mode [15]. These parameters correspond to a fiber similar to a 300 meter long hollow single-mode fiber produced by Sudo et $al.$ [16].

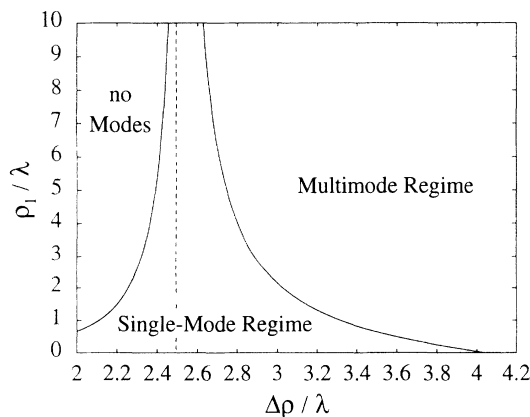For these parameters we solved the eigenvalue problem

TABLE I. Hollow fiber parameters.

Parameter	Value
Refractive index of the annular core n_F	1.500
Refractive index of the cladding n_{Cl}	1.497
Hole radius over wavelength ρ_1/λ	2.889
Core thickness over wavelength $\triangle\rho/\lambda$	2.889

and found $\bar{\beta}_{11} = 0.049$. The electric field can be written in the form

$$\boldsymbol{E}(r,\phi,z) = \mathcal{E}(r)\boldsymbol{\epsilon}(\phi)e^{i(\phi+\beta z - \omega t)} + c.c., \tag{8}$$

with $\mathcal{E}(r)$ a real positive function depending only on the radius and $\boldsymbol{\epsilon}(\phi)$ a complex unit vector. A plot of the function $\mathcal{E}$ (Fig. 3) shows that the evanescent wave is limited to a small region close to the wall. Since $U = 20.2$ the Bessel functions in (5) can be expanded for large arguments giving the following approximation to $\mathcal{E}$ in the evanescent wave (region I):

$$\mathcal{E}(r) \approx \mathcal{E}_0 \exp\left(\frac{U(r-\rho_1)}{\rho_1}\right). \tag{9}$$

$\mathcal{E}_0$ depends on the power P guided along the fiber of Table I according to

$$\mathcal{E}_0 = 1.51 \times 10^4 \frac{1}{\lambda\,(\mu m)} \sqrt{\frac{P\,(mW)}{10}} \quad (V\,m^{-1}). \tag{10}$$

Using spherical unit vectors $\boldsymbol{e}_\pm = \mp\frac{1}{\sqrt{2}}(\hat{\boldsymbol{x}}\pm i\hat{\boldsymbol{y}})$ and $\boldsymbol{e}_z = \hat{\boldsymbol{z}}$, the polarization vector $\boldsymbol{\epsilon}$ is found to be

$$\boldsymbol{\epsilon}(\phi) = \omega_+ ie^{-i\phi}\boldsymbol{e}_+ + \omega_0\boldsymbol{e}_z + \omega_- ie^{i\phi}\boldsymbol{e}_-, \tag{11}$$

with the parameters $\omega_+ = 0.90$, $\omega_0 = 0.45$, and $\omega_- = 1.9 \times 10^{-2}$.

FIG. 2. Map of the various modal structure regimes in the ρ_1-$\triangle\rho$ plane. All points above the solid line correspond to a configuration which either is multimode or possesses no (unattenuated) modes at all. The dashed line indicates the cutoff for the TE_1 modes of the asymmetric slab. Refractive indices are the same as in Table I.
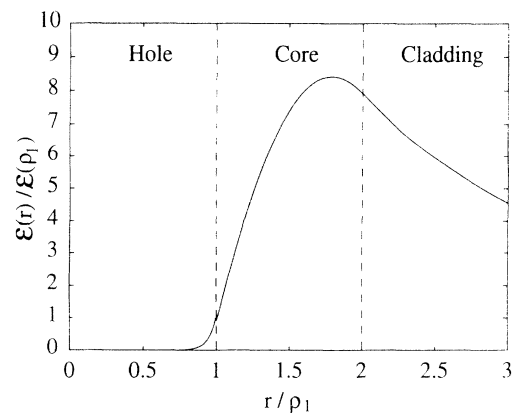

FIG. 3. Electric field strength $\mathcal{E}(r)$ for the HE_{11} mode vs radius r for the parameters of Table I.

III. QUANTIZED ATOMIC MOTION IN THE FIBER

In this section we will derive an approximate expression for the eigenstates of the center-of-mass motion for atoms confined by the evanescent field to the interior of the hollow fiber.

The simplest realistic model for an atom inside the fiber is a two-level system with a nondegenerate ground state (angular momentum $J_g=0$) and an excited state ($J_e=1$) with Zeeman substructure. The notation for the various levels is given in Fig. 4. The evanescent field will be treated classically. Since we only want to study the *coherent* propagation of atoms along the fiber we do not consider the state of the atom after a spontaneous emission. Hence we only need to calculate the wave function without any photons spontaneously emitted into the quantized electromagnetic field vacuum. This is the first term in the expansion [17]

$$|\Psi(t)\rangle = \left\{ |\psi_g(t)\rangle \otimes |g\rangle \right.$$
$$\left. + \sum_{j=\pm,0} |\psi_j(t)\rangle \otimes |j\rangle e^{-i\omega t} \right\} \otimes |\text{vac}\rangle + \cdots, \quad (12)$$

where j labels the Zeeman sublevels. The motion of the atom along the fiber decouples from the transverse motion for a straight fiber. Hence it is convenient to represent the center-of-mass wave functions $|\psi_\gamma\rangle$ in an eigenbasis of the complete set of commuting observables $\{X, Y, P_z\}$, i.e., $\psi_\gamma(x,y,p_z,t) = \langle x,y,p_z|\psi_\gamma(t)\rangle$. Using (8) and (11), we can write the dipole interaction with the classical field as

$$\boldsymbol{d} \cdot \boldsymbol{E}_c(\boldsymbol{x},t) = \sum_{j=\pm,0} \tilde{\Omega}_j(x,y) A_j^\dagger e^{i(\beta z - \omega t)} + \text{H.c.}, \quad (13)$$

where

$$\tilde{\Omega}_+(x,y) = d\mathcal{E}(r)\omega_+ i, \quad (14a)$$
$$\tilde{\Omega}_0(x,y) = d\mathcal{E}(r)\omega_0 e^{i\phi}, \quad (14b)$$
$$\tilde{\Omega}_-(x,y) = d\mathcal{E}(r)\omega_- i e^{2i\phi}. \quad (14c)$$

Here $A_j = |g\rangle\langle j|$ are the atomic lowering operators and d is the dipole moment of the transition (d incorporates the Clebsch-Gordon coefficients, which are all equal to 1). Making use of the fact that the z dependence of the dipole interaction (13) is $e^{i\beta z}$, which corresponds to a
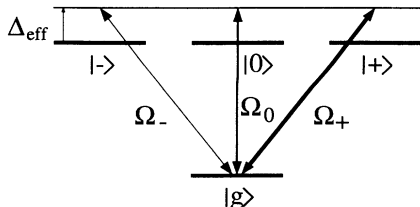

FIG. 4. Atomic level scheme. The line thickness of the various transitions indicates their strength in the field of Eqs. (8) and (11).

translation in the P_z representation, we find the equation of motion, in the rotating wave approximation, [17]

$$i\hbar \frac{\partial}{\partial t} \psi_\gamma(x,y,p_\gamma,t) = \sum_{\nu=g,\pm,0} (H_{\text{eff}})_{\gamma\nu} \psi_\nu(x,y,p_\nu,t) \quad (15)$$

with

$$(H_{\text{eff}})_{\gamma\nu} = \left(-\frac{\hbar^2}{2M}\nabla_t^2 + \frac{(p_z + \hbar\beta)^2}{2M} - \hbar\Delta \right) \delta_{\gamma,\nu}$$
$$- i\frac{\hbar\kappa}{2}(1 - \delta_{\gamma 1}) + \mathbf{V}_{\gamma\nu}, \quad (16)$$

and $\gamma, \nu = g, \pm, 0$. Here κ is the spontaneous decay rate, δ is the Kronecker symbol, $p_g = p_z$ is the z component of the momentum of the atom in the ground state, $p_{\pm,0} = p_z + \hbar\beta$ is the momentum of the atom in the excited states (including the additional momentum due to the absorption of a photon from the laser field), and $\Delta = \omega - \omega_A$ is the atom-laser detuning. We define $\hat{\Delta}_{\text{eff}} = \Delta - p_z\beta/M - \hbar^2\beta^2/2M$, the effective detuning including a Doppler shift due to the atomic motion and a recoil shift. The coupling between the states is then given by

$$\mathbf{V} = \begin{pmatrix} \hbar\Delta_{\text{eff}} & -\tilde{\Omega}_+^*(x,y) & -\tilde{\Omega}_0^*(x,y) & -\tilde{\Omega}_-^*(x,y) \\ -\tilde{\Omega}_+(x,y) & 0 & 0 & 0 \\ -\tilde{\Omega}_0(x,y) & 0 & 0 & 0 \\ -\tilde{\Omega}_-(x,y) & 0 & 0 & 0 \end{pmatrix}, \quad (17)$$

where we use the ordering $\{g, +, 0, -\}$. The Schrödinger equation (15) has the property that it only couples the ground state with momentum p_z to the excited states with momentum $p_z + \hbar\beta$. Therefore the momentum p_z plays the role of a parameter and will be omitted in the following.

The next step is to transform to an adiabatic basis [18], obtained by diagonalizing $\mathbf{V}(x,y)$ for each x,y. Using the notation

$$\Omega_R(r) = \sqrt{[d\mathcal{E}(r)]^2 + \left(\frac{\hbar\Delta_{\text{eff}}}{2}\right)^2}, \quad (18)$$

we find the eigenvalues are $V_{1,2}(r) = \hbar\Delta_{\text{eff}}/2 \pm \Omega_R(r)$ (the plus sign refers to the adiabatic state n_1 and the minus sign to n_2) and $V_{3,4} = 0$. The corresponding eigenvectors are

$$\boldsymbol{n}_{1,2}(r,\phi) = N_{1,2}(r) \begin{pmatrix} \hbar\Delta_{\text{eff}}/2 \pm \Omega_R(r) \\ -\tilde{\Omega}_+(r,\phi) \\ -\tilde{\Omega}_0(r,\phi) \\ -\tilde{\Omega}_-(r,\phi) \end{pmatrix} \quad (19)$$

and

$$\boldsymbol{n}_3(\phi) = N_3 \begin{pmatrix} 0 \\ 0 \\ i\omega_- e^{-2i\phi} \\ \omega_0 e^{-i\phi} \end{pmatrix}, \boldsymbol{n}_4(\phi) = N_4 \begin{pmatrix} 0 \\ \omega_0^2 + \omega^2 \\ i\omega_0\omega_+ e^{i\phi} \\ -\omega_-\omega_+ e^{2i\phi} \end{pmatrix}. \quad (20)$$

The latter two possess no admixture of the ground state and therefore represent purely excited states. $N_1, \ldots, N_4$

are normalization constants. Note that the eigenvalues are functions only of the radial coordinate r. This fact considerably simplifies the calculation of the atomic eigenstates as will be shown later. Expanding $\psi = (\psi_g, \psi_+, \psi_0, \psi_-)$ in the adiabatic basis,

$$\psi(x, y, t) = \sum_{\gamma=1}^{4} \alpha_\gamma(x, y, t) e^{-i\omega_p t} n_\gamma(x, y), \qquad (21)$$

where $\hbar\omega_p = (p_z + \hbar\beta)^2/2M - \hbar\Delta_{\text{eff}}$, we deduce from (15)

$$i\hbar\frac{\partial}{\partial t}\alpha_\gamma = \sum_{\nu=1}^{\mu}\left(\mathbf{H}_{\gamma\nu}^{\text{ad}} + \mathbf{V}_{\gamma\nu}^{\text{na}} - \frac{i\hbar}{2}\mathbf{\Gamma}_{\gamma\nu}\right)\alpha_\nu, \qquad (22)$$

where

$$\mathbf{H}_{\gamma\nu}^{\text{ad}} = \left(-\frac{\hbar^2}{2M}\nabla_t^2 + V_\gamma(r)\right)\delta_{\gamma\nu} \qquad (23)$$

is the adiabatic Hamiltonian,

$$\mathbf{V}_{\gamma\nu}^{\text{na}} = -\frac{\hbar^2}{2M}\sum_{\sigma=1}^{4}\left[n_{\gamma\sigma}^*\left(\nabla_t^2 n_{\nu\sigma}\right) + 2n_{\gamma\sigma}^*(\nabla_t n_{\nu\sigma} \cdot \nabla_t)\right] \qquad (24)$$

describes the nonadiabatic coupling between the adiabatic states [18], and

$$\mathbf{\Gamma} = \kappa\begin{pmatrix} N_1^2(d\mathcal{E})^2 & N_1 N_2(d\mathcal{E})^2 & 0 & 0 \\ N_1 N_2(d\mathcal{E})^2 & N_2^2(d\mathcal{E})^2 & 0 & 0 \\ 0 & 0 & 1 & 0 \\ 0 & 0 & 0 & 1 \end{pmatrix} \qquad (25)$$

is the damping due to spontaneous emission. In Eq. (24) $n_{\nu\sigma}$ denotes the σth component of the vector n_ν. The adiabatic Hamiltonian (23) governs the evolution of a wave packet, prepared in one of the adiabatic states (or a superposition of them), in the corresponding adiabatic potentials V_γ. A plot of these adiabatic potentials is given in Fig. 5. It is easy to see that we need a blue detuning, i.e., $\Delta_{\text{eff}} > 0$, for the confinement of ground state atoms.
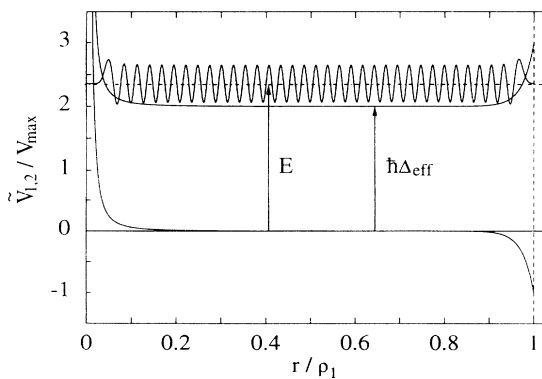

FIG. 5. Schematic plot of a typical wave function in the confining potential $\tilde{V}_1$. The dashed line on the right represents the hole-core interface. The attractive potential $\tilde{V}_2$ is also plotted, but the separation between the two potentials is understated.

In this case, the adiabatic state which converges to the ground state in the limit $\mathcal{E} \to 0$ is n_1 and the confining potential is V_1.

It is clear from (22) that there are three processes that limit the confinement of particles inside the fiber. The first is loss due to spontaneous emission. Since all adiabatic states and particularly the state n_1 have admixtures of excited internal states, there is a nonzero probability for them to decay to an untrapped state. We introduce the parameter η, proportional to the ratio of the Rabi frequency to the detuning,

$$\eta = 2d\mathcal{E}_0/\hbar\Delta_{\text{eff}}. \qquad (26)$$

The probability of the atom being excited increases with η. From (25) and (19) we deduce that Γ_{11} is a monotonically decreasing function of the detuning. In particular, Γ_{11} has a series expansion in η

$$\Gamma_{11} = \kappa e^{2U(r-\rho_1)/\rho_1}\frac{\eta^2}{4} + O(\eta^4). \qquad (27)$$

This is just the spontaneous emission rate times the probability for the atom to be in its excited state. Similarly the confining potential V_1 can be expanded

$$V_1(r) = \hbar\Delta_{\text{eff}}\left(1 + \frac{\eta^2}{4}e^{2U(r-\rho_1)/\rho_1}\right) + O(\eta^4). \qquad (28)$$

In the following we assume $\eta/2 \ll 1$ so that these expansions can be used.

A second loss process is the tunneling of the atoms to the wall. In this case the atoms will stick to the wall or will be scattered from it, leading to a loss of coherence. We assume here that all these particles are lost from the coherent transport. So far we have neglected any interaction between the atoms and the wall (Casimir-Polder force [19]). In Sec. IV D we will estimate its magnitude and discuss its influence on the guidance of atoms. The third loss mechanism is due to the nonadiabatic transitions to the nonconfining adiabatic potentials. We will estimate the magnitude of the three loss mechanisms in Sec. IV.

We next consider the atomic center-of-mass eigenstates of atoms in the adiabatic state n_1 under the assumption of negligible losses. A confined atomic wave function of the form (21) can only have an α_1 component. Exploiting the radial symmetry of our problem, we can write the eigenstates as simultaneous eigenvectors of $\mathbf{H}^{\text{ad}}$ and the z component of the angular momentum operator L_z

$$\alpha_1(r, \phi) = \frac{\tilde{\alpha}_1(r)}{\sqrt{r}}e^{im\phi}, \qquad (29)$$

with $m = 0, \pm 1, \dots$. The eigenvalue equation for $\tilde{\alpha}_1$ is

$$\left(-\frac{\hbar^2}{2M}\frac{d^2}{dr^2} + \tilde{V}_1(r)\right)\tilde{\alpha}_1(r) = E\tilde{\alpha}_1(r) \qquad (30)$$

with the potential

$$\tilde{V}_1(r) = V_1(r) + \frac{\hbar^2}{2M}\frac{m^2 - \frac{1}{4}}{r^2}, \qquad (31)$$

including the centrifugal barrier. To be rigorous, we

should write $\tilde{\alpha}_{1Em}$, but we will suppress the indices E and m for simplicity of notation. We will calculate the eigenfunctions in a WKB approximation. Using a Langer transformation [20] to avoid difficulties with WKB solutions in the vicinity of the origin, we can write the nth bound eigenfunction in terms of Airy functions as [20]

$$\tilde{\alpha}_1 = \begin{cases} c \left| \sigma_{1-}/k_1^2 \right|^{1/4} \mathrm{Ai}(\sigma_{1-}) & \text{for } r < r_+ - \epsilon \\ (-1)^n c \left| \sigma_{1+}/k_1^2 \right|^{1/4} \mathrm{Ai}(\sigma_{1+}) & \text{for } r > r_- + \epsilon \end{cases}$$

(32)

with the wave number

$$k_1(r) = \sqrt{\frac{2M}{\hbar^2} \left| E - V_1(r) - \frac{\hbar^2 m^2}{2M} \frac{1}{r^2} \right|}$$

(33)

and

$$\sigma_{1\pm}(r) = \pm \mathrm{sgn}(r - r_\pm) \frac{3}{2} \left| \int_{r_\pm}^r dr' k_1(r') \right|^{2/3}.$$

(34)

We denote the normalization constant by c. Equation (32) is a uniform WKB approximation which is also valid in the vicinity of the classical turning points for small and large r, denoted by r_- and r_+, respectively. They are defined by $k_1(r_\pm) = 0$ for $m \neq 0$ and by $r_- = 0$ and $k_1(r_+) = 0$ for $m = 0$. The WKB approximation is valid provided the energy of the state is considerably larger than the ground state energy and provided the de Broglie wavelength is smaller than the decay length of the evanescent field. The WKB quantization condition on the phase integral $L(E)$ is

$$L(E) = \int_{r_-}^{r_+} dr' k_1(r') = \left(n + \frac{1}{2} \right) \pi, \quad n = 0, 1, 2, \ldots,$$

(35)

which determines E by ensuring that the approximate solutions (32) match in the overlap region, where both are valid. A picture of a typical wave function is shown in Fig. 5. The quantity ϵ in (32) excludes a small region around the classical turning points, where one or the other of the two lines in the approximation (32) breaks down (the uniform WKB solution can only handle a single turning point).

There is no analytical expression for the indefinite integral in (34), but we can find a good approximation by making use of the short range of the Stark-shift potential V_1 and the long range of the centrifugal barrier. Let r_p be a point below which the potential $V_1(r)$ can be neglected [for example, $r_p \approx \rho_1(1 - 2/U) \approx 0.9\rho_1$]. If we neglect the exponential part in $\tilde{V}_1(r)$ for $r < r_p$ and approximate the centrifugal barrier by the constant value $\hbar^2 m^2/2M\rho_1^2$ for $r > r_p$, then the resulting integral is analytically soluble and depends only very weakly on the choice of r_p.

We can use this approximation to derive an analytical expression for the phase integral. It is convenient to introduce the quantity

$$\epsilon_R = \hbar^2 U^2/2M\rho_1^2.$$

(36)

Since U/ρ_1 is on the order of β [cf. (6a)], ϵ_R is of the order of the recoil energy $\hbar^2 k^2/2M$. We denote the (center-of-mass) energy of the atom relative to the bottom of the potential $V_1 + \hbar^2 m^2/2Mr^2$ by

$$E_k = E - \hbar\Delta_{\mathrm{eff}} - \hbar^2 m^2/2M\rho_1^2.$$

(37)

We find

$$L(E) = \sqrt{\frac{\epsilon_R}{E_k}} \frac{m^2}{U} - \frac{m\pi}{2} + \sqrt{\frac{E_k U^2}{\epsilon_R} - m^2}$$

$$\times \left[1 - \frac{1}{U} + \frac{1}{U} \ln \left(2\sqrt{\frac{E_k}{V_{\mathrm{max}}} - \frac{\epsilon_R m^2}{V_{\mathrm{max}}} U^2} \right) \right].$$

(38)

Assuming $E_k/\epsilon_R \gg m^2/U^2$ and $\ln(2\sqrt{E_k/V_{\mathrm{max}}}) \ll U$, we can simplify (38) to give

$$L(E) \approx U\sqrt{\frac{E_k}{\epsilon_R}} - \frac{m\pi}{2}.$$

(39)

Another application of this approximation is to derive an analytical estimate of the normalization constant c. From Fig. 5 it can be seen that up to a small error we can neglect the exponentially decaying parts of the wave function beyond the classical turning points, replace the slowly modulated part of the wave function by its average over one period, and use the preceding approximation for the resulting integral. We find

$$c \approx \sqrt{k_1(r_p)/\rho_1}.$$

(40)

We will use both of these results in the next section to calculate the loss rates from the confined eigenstate.

IV. LOSS MECHANISMS

In this section we will derive approximate analytical expressions for the three loss mechanisms identified in the preceding section. We assume that these loss rates are sufficiently small that they can be investigated separately. The Casimir-Polder interaction of the atom with the wall of the fiber is considered in Sec. IV D.

A. Spontaneous emission

A system governed by the non-Hermitian Hamiltonian

$$H_{\mathrm{eff}} = H - \frac{i}{2}\hbar\Gamma$$

(41)

where both H and Γ are Hermitian, does not conserve the norm of the state vector $|\chi(t)\rangle$. It is easy to show that

$$\frac{d}{dt}\langle \chi(t)|\chi(t)\rangle = -\langle \chi(t)|\Gamma|\chi(t)\rangle,$$

(42)

MARKSTEINER, SAVAGE, ZOLLER, AND ROLSTON

which corresponds to a loss of probability with rate $\langle \chi(t)|\Gamma|\chi(t)\rangle$.

In our particular case, $|\chi(t=0)\rangle$ is a stationary state α_1 of the atom in the adiabatic state n_1. The spontaneous emission loss rate is therefore given by

$$L_{\rm sp} = 2\pi \int_0^{\rho_1} dr |\tilde{\alpha}(r)|^2 \Gamma_{11}(r). \qquad (43)$$

In the following we will denote the height of the potential barrier V_1 Eq. (28) at the wall by $V_{\rm max} = \hbar\Delta_{\rm eff}\eta^2/4$. Employing the same approximation we used in deriving (38), we find that

$$\frac{2}{3}\sigma_{1+}(r)^{3/2} = \frac{1}{2}\sqrt{E_k/\epsilon_R}\ f\left(\frac{2U}{\rho_1}(r-r_+)\right), \qquad (44)$$

where $f(x) = \int_0^x dy\sqrt{|1-e^y|}$. This allows us to write (43) for well bound states [i.e. $|\tilde{\alpha}(\rho_1)|^2 \ll |\tilde{\alpha}(r_+)|^2$] in the form

$$L_{\rm sp} = \frac{\kappa\eta^2}{4U}\frac{E_k}{V_{\rm max}}K\left(\sqrt{E_k/\epsilon_R}\right) \qquad (45)$$

with

$$K(x) = \pi\left(\frac{3}{4}x\right)^{1/3}\int_{-\infty}^{+\infty} dy\ \frac{|f(y)|^{1/3}e^y}{\sqrt{|1-e^y|}}$$
$$\times {\rm Ai}^2([\tfrac{3}{4}xf(y)]^{\frac{2}{3}}). \qquad (46)$$

A plot of the function $K(x)$ is shown in Fig. 6. For $\sqrt{E_k/\epsilon_R} \gg 1$ it converges to unity. The energy of the ground state can be estimated from that of a particle confined inside a circle to be $x = \sqrt{E_k/\epsilon_R} \approx 2.4/U$ [10]. Since the WKB approximation for the wave functions is only valid for energies considerably larger than the ground state energy, a lower bound for the validity of (45) is $x \approx 10/U$.

The expression (45) with $K \equiv 1$ is identical to the loss rate for a *classical* particle moving with energy E_k in the potential

$$V(r) = \hbar\Delta_{\rm eff}e^{2U(r-\rho_1)/\rho_1}\eta^2/4 + \hbar^2m^2/2Mr^2 \qquad (47)$$
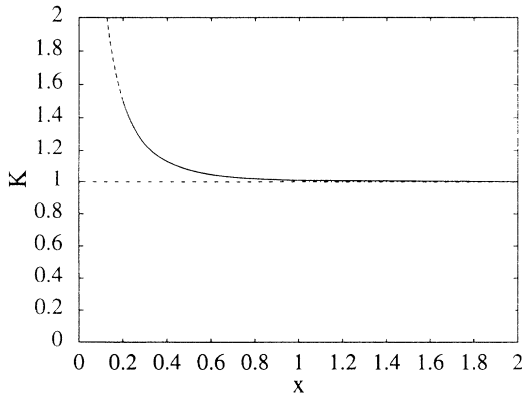
and experiencing a local loss rate (27).

FIG. 6. Plot of the function $K(x)$, Eq. (46). For small x the WKB approximation is not valid (dashed line), although formally $K(x)$ can still be evaluated.

B. Tunneling

In the case of small tunneling probability, the tunneling loss rate is given by [21]

$$L_T = e^{-2\theta}\left(\hbar\frac{\partial L}{\partial E}\right)^{-1}. \qquad (48)$$

Here L is the phase integral [Eq. (35)] and $\theta = \int_{r_+}^{\rho_1} dr k_1(r)$ is the tunneling integral. The exponential factor represents the tunneling probability per bounce and the term in large parentheses gives the number of reflections per unit time. Using the approximations described in Sec. III we find

$$L_T = \frac{2\epsilon_R}{\hbar U}\sqrt{\frac{E_k}{\epsilon_R}}\exp\left[-2\sqrt{\frac{V_{\rm max}}{\epsilon_R}}\ g\left(\frac{E_k}{V_{\rm max}}\right)\right] \qquad (49)$$

with

$$g(x) = \sqrt{x}\left(\sqrt{\frac{1}{x}-1}-\arctan\sqrt{\frac{1}{x}-1}\right). \qquad (50)$$

An important property of the tunneling loss rate is its exponential behavior as a function of $E_k/V_{\rm max}$. In most cases of interest, the potential height $V_{\rm max}$ is much larger than the recoil energy, which leads to a large factor in the exponent and therefore to a very sharp onset of tunneling. Due to this exponential behavior compared to the linear behavior of spontaneous emission losses with energy, the switching from one to the other being the dominant loss is decisive.

C. Nonadiabatic transitions

The first step in the calculation of the nonadiabatic losses is the expansion of $\mathbf{V}^{\rm na}$ in the small parameter η, Eq. (26). From this expansion we deduce conditions which have to be fulfilled to consider $\mathbf{V}^{\rm na}$ a small perturbation. Using Fermi's golden rule to calculate the transition rate to the attracted adiabatic state n_2, we can estimate the loss rate.

In our case, we want to calculate the transition rate from the confined state $(\alpha_1, 0, 0, 0)$ to the other adiabatic states, which are either attracted or not affected by the evanescent light field. Therefore we only need to know the components $\mathbf{V}_{\gamma\nu}^{\rm na}$ with $\nu = 1$. The expansion of $\mathbf{V}_{\gamma 1}^{\rm na}$ in the small parameter η up to order η^1 is found after some calculation to posses only a component

$$\mathbf{V}_{21}^{\rm na} = -\epsilon_R\frac{\eta}{2}e^{U(r-\rho_1)/\rho_1}\left(1+\frac{2\rho_1}{U}\frac{\partial}{\partial r}\right) \qquad (51)$$

if we neglect the small coupling (of order $\omega_-/\omega_{0,+} \ll 1$) to the other two adiabatic potentials. The conditions for $\mathbf{V}^{\rm na}$ being a small perturbation of the adiabatic Hamiltonian for the ground state are therefore

$$\frac{\epsilon_R}{\hbar\Delta_{\rm eff}} \ll \frac{\eta}{2}, \qquad \frac{2\epsilon_R}{\hbar\Delta_{\rm eff}}\sqrt{\frac{E_k}{\epsilon_R}} \ll \frac{\eta}{2}. \qquad (52)$$

We are able to use a WKB approximation for the wave function in the second adiabatic potential $\tilde{V}_2(r)$

$$\alpha_2(r, \phi) = \frac{\tilde{c} \, e^{i\tilde{m}\phi}}{\sqrt{rk_2(r)}} \cos\left(\int_{\hat{r}_-}^{r} dr' k_2(r') - \frac{\pi}{4}\right), \quad (53)$$

where $\tilde{c} = \sqrt{M}/\pi\hbar$, $k_2(r) = [2M|E - \tilde{V}_2(r)|/\hbar^2]^{1/2}$, and $\hat{r}_-$ denotes the classical turning point in the potential $\tilde{V}_2$. Due to the assumption $\eta/2 \ll 1$, this is a rapidly oscillating function of r.

Since the nonadiabatic loss rate is given by $L_{na} \approx (2\pi/\hbar)|\langle f|\mathbf{V}_{21}^{na}|i\rangle|^2$, where $|i\rangle$ is the confined initial state and $|f\rangle$ is the attracted final state, we are interested in the quantity $|\langle f|\mathbf{V}_{21}^{na}|i\rangle|$. A well-known inequality from elementary calculus allows us to exchange the absolute value with the integration

$$|\langle f|\mathbf{V}_{21}^{na}|i\rangle| = \left|\int_0^\infty dr'r' \int_0^{2\pi} d\phi \, \alpha_2^*(r', \phi)\mathbf{V}_{21}^{na}\alpha_1(r', \phi)\right|$$

$$\leq \int_0^\infty dr' 2\pi r' \left|\frac{\tilde{\alpha}_2(r')}{\sqrt{r'}}\mathbf{V}_{21}^{na}\frac{\tilde{\alpha}_1(r')}{\sqrt{r'}}\right|. \quad (54)$$

Note that since $\mathbf{V}_{21}^{na}$ does not depend on the angle ϕ, the state α_1 couples only to states α_2 with the same angular momentum m. The function under the first integral resembles a slowly modulated cosine and therefore most of the contributions cancel each other. On the other hand, the second integrand is always positive and different half waves do not cancel each other, but add up. Therefore we expect the second integral to be a gross overestimate. The rapid oscillations of $\tilde{\alpha}_2(r')$ allow us to replace this function by its average value. To derive an upper bound for the remaining integral we use the fact that a derivative of $\tilde{\alpha}_1(r')/\sqrt{r'}$ with respect to r' is on the order of $k_1\tilde{\alpha}_1/\sqrt{r'}$. Therefore we can replace $\mathbf{V}_{21}^{na}\tilde{\alpha}_1(r')/\sqrt{r'}$ by its upper bound

$$\left|\mathbf{V}_{21}^{na}\frac{\tilde{\alpha}_1(r')}{\sqrt{r'}}\right| \leq \epsilon_R \frac{\eta}{2} e^{U(r'-\rho_1)/\rho_1}\left(1 + \frac{2\rho_1 k_1}{U}\right)\frac{|\tilde{\alpha}_{1max}|}{\sqrt{r'}}. \quad (55)$$

The quantity $|\tilde{\alpha}_{1max}|$ can be estimated from (32) and (40)to be $1/\sqrt{\pi\rho_1}$, since $Ai(x) < 1/\sqrt{\pi}$. Also the 1 in the large parentheses in (55) can be neglected in comparison to the second term (for all but the lowest few states). We hence find the upper bound to be

$$L_{na} \ll 6.5\frac{\epsilon_R}{\hbar}\frac{\eta^2}{4}\frac{\rho_1 k_1^2}{U^2 k_2}. \quad (56)$$

If we compare this loss rate with the loss due to spontaneous emission, we find

$$\frac{L_{na}}{L_{sp}} \ll 1.6\eta^2\frac{\Delta_{eff}}{\kappa}\sqrt{\frac{\epsilon_R}{\hbar\Delta_{eff}}}. \quad (57)$$

As will be discussed in Sec. V, this shows that the non-adiabatic transitions are negligible in comparison with the spontaneous emission for $\eta/2 \ll 1$.

D. Casimir-Polder forces

In this subsection we give a semiquantitative discussion of the interaction between the atom and the wall of

the hollow fiber, which we have neglected so far. This Casimir-Polder (CP) force lowers the effective potential barrier seen by the atom. Hence it will move the trade-off between tunneling and spontaneous emission losses toward a higher Stark-shift barrier and lower detunings. The CP force becomes significant at distances from the wall where the evanescent field becomes strong. Its origin is the modification of the polarization and spectral densities of the quantized electromagnetic field vacuum due to the presence of the dielectric waveguide. This modification leads to a spatially varying Lamb shift and hence to a force [19]. Since the calculation of this Casimir-Polder force for our geometry is extremely involved, we restrict ourselves to a simple estimate.

For a spherical ground state atom between parallel metallic plates, the position-dependent Lamb shift is given by [22,23]

$$U_{CP}(r) = -\sum_e \frac{\pi|d_{eg}|^2}{6\varepsilon_0(2\rho_1)^3}\int_0^\infty d\xi\, \xi^2 \frac{\cosh(\pi\xi r/\rho_1)}{\sinh(\pi\xi)}$$

$$\times \arctan\left(\frac{\xi\lambda}{4\rho_1}\right), \quad (58)$$

where the sum runs over all excited states, d_{eg} is the dipole matrix element between the ground and excited states, and $2\rho_1$ is the separation of the metallic plates. This force has been measured experimentally [22].

In our case Eq. (58) overestimates the force between the atoms and the wall for two reasons. First, the walls are not metallic but purely dielectric, so the modification of the electromagnetic fields is less than in the metallic case. We account for this effect by introducing an additional factor [24]

$$(n_F^2 - 1)/(n_F^2 + 1) \approx 0.38 \quad (59)$$

into Eq. (58). Second, we have a circular geometry. It is reasonable to expect a decrease of the CP force analogous to the decrease of the van der Waals force (which is a limiting case of the former) an atom experiences from its mirror image, which is farther away for the curved mirror. Since no estimate of this effect exists so far, we will neglect it.

The CP potential, calculated from (58) and including the factor (59), is plotted as a function of the radius in Fig. 7 for cesium and sodium. The resulting force is attractive and diverges as the atom approaches the surface. Therefore, the total potential for the atomic motion, i.e., the Stark-shift potential plus the CP potential, is significantly lowered and becomes attractive close to the wall. In the case of sodium, a potential barrier of $2000\epsilon_R$ is reduced to about $800\epsilon_R$ and a potential barrier of $200\epsilon_R$ is decreased to about $30\epsilon_R$. For potential heights below about $30\epsilon_R$ no repulsive barrier is left. In the following section we will find that some of this reduced barrier height can be recovered by decreasing the detuning, at the expense of increased spontaneous emission.

With the addition of the CP potential the integrals for the spontaneous emission loss rate L_{sp}, Eq. (43), and tunneling loss rate L_T, Eq. (48), must be evaluated numerically.
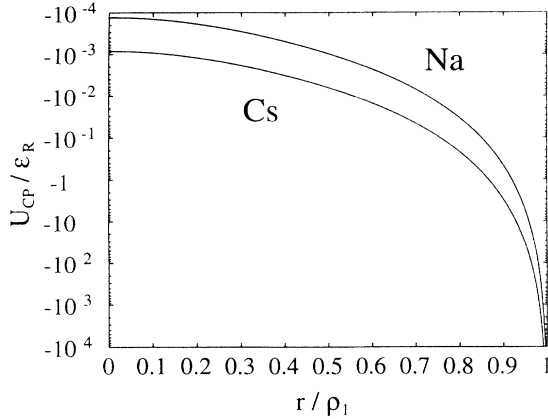
FIG. 7. Casimir-Polder force for Cs and Na, calculated using Eqs. (58) and (59).

V. DISCUSSION

We now use the preceding theory to discuss the feasibility of hollow fiber atomic waveguides. We will not address the issue of how to efficiently launch light and atoms into them. Rather we shall estimate the range of transverse atomic kinetic energies that might reasonably be guided through meter length straight fibers.

As discussed in Sec. IV, guidance is limited by three loss mechanisms: spontaneous emission, tunneling to the waveguide's walls, and nonadiabatic transitions to unconfined states. Close to resonance the confining force is stronger so tunneling is reduced; however, spontaneous emission is increased. Hence the atom-laser detuning can be chosen to optimize the combined losses due to spontaneous emission and tunneling. The detunings are then usually sufficiently high that nonadiabatic transitions are negligible.

In the following we determine the conditions for optimal guidance of either Na or Cs atoms. We consider a hollow fiber having the parameters of Table I. We also fix the laser power guided by the optical fiber to be 10 mW. This is chosen as a reasonably achievable value. The corresponding maximum evanescent electric field is given by Eq. (10). The remaining free parameter is the atom laser detuning Δ, which we represent using the dimensionless ratio (26) $\eta = 2d\mathcal{E}_0/\hbar\Delta_{\text{eff}}$. For a fixed total loss rate we shall find the value of η that maximizes the confined transverse kinetic energy.

We assume that the nonadiabatic loss rate is negligible, which can be verified at the end of the calculation. The total loss rate is the sum of the spontaneous emission loss rate L_{sp}, Eq. (45), and the tunneling loss rate L_T, Eq. (49). For a fixed total loss rate $L_{\text{max}} = L_T + L_{\text{sp}}$, the transverse kinetic energy E_k can be found as a function of η. The optimal η giving the maximum transverse kinetic energy $E_{k\text{max}}$ can then be found.

The results are presented in Figs. 8 and 9. The solid lines ignore the Casimir-Polder potential while the dashed lines include it, following Sec. IV D. Figure 8 shows the value of η which maximizes the confined transverse kinetic energy for a fixed value of the total loss rate.
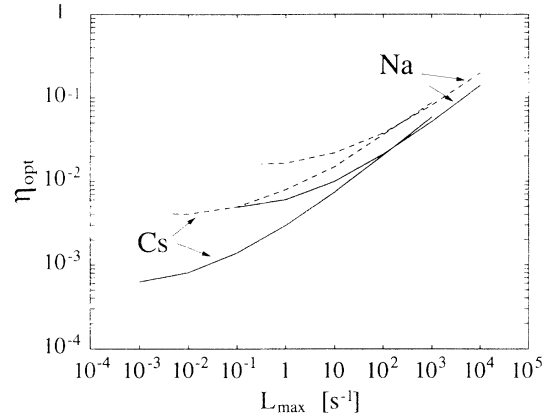

FIG. 8. Optimal η [Rabi frequency over effective detuning Eq. (26)] vs maximum loss rate. The solid curves ignore the Casimir-Polder effect. The dashed curves include a modified potential barrier according to Eqs. (58) and (59). The fiber has the parameters of Table I and guides 10 mW of power.

Figure 9 shows the associated maximum confined transverse kinetic energy $E_{k\text{max}}$. We plot the ratio of $E_{k\text{max}}$ to ϵ_R [Eq. (36)]. This is because ϵ_R is approximately the recoil energy and hence gauges the difficulty of laser cooling the transverse atomic velocity.

Figure 8 shows that the minimum achievable loss rate for Cs is several orders of magnitude smaller than for Na. This is a result of the larger dipole moment and lower spontaneous emission rate for Cs; see Table II. The much higher ratio of maximum confined energy to recoil energy for Cs in Fig. 9 is additionally a result of its lower recoil velocity, due to its higher mass and lower transition frequency.

From Fig. 9 the smallest value of $\sqrt{E_k/\epsilon_R}$ is about 0.5 and we are therefore justified in using the approximation $K \approx 1$ in evaluating the spontaneous emission loss rate (45). The inequalities used to derive the tunneling loss rate (49) are also fulfilled, provided that the angular momentum quantum number m is not too large (cf. the end
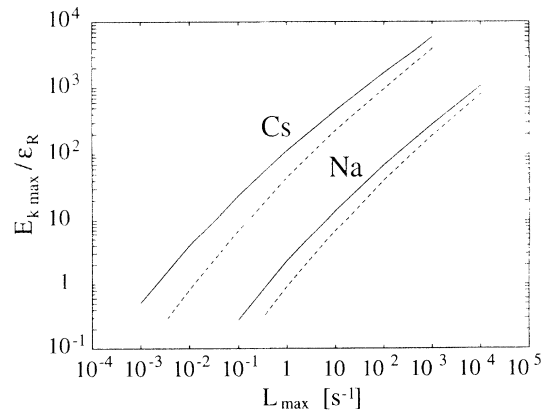

FIG. 9. Maximum guided energy vs maximum loss rate. The solid curves ignore the Casimir-Polder effect. The dashed curves include a modified potential barrier according to Eqs. (58) and (59). The fiber has the parameters of Table I and guides 10 mW of power.

TABLE II. Atomic parameters for cesium and sodium.

Element	M (kg)	λ (nm)	d ($C\,m^2$)	κ (MHz)
Cs	2.29×10^{-25}	852	2.5×10^{-29}	$2\pi\times5$
Na	3.82×10^{-26}	589	2.0×10^{-29}	$2\pi\times10$

of Sec. III). Finally the adiabatic loss rate is negligible since the largest value for the upper bound Eq. (57) is $L_{na}/L_{sp}\ll6\times10^{-2}$, found for the largest maximum loss rate of Na.

We have obtained formulas for the loss rates per unit time L_{max}. The transmission loss R through a length l of fiber is then inversely proportional to the velocity of the atoms through the fiber $v_{\parallel}$: $R=lL_{max}/v_{\parallel}$. We consider two extreme cases for $v_{\parallel}$: the uncooled case $v_{\parallel}=1000$ m s^{-1}, corresponding to an uncooled atomic beam, and a cooled case $v_{\parallel}=1$ m s^{-1}, corresponding to cooling near the (Na) Doppler limit. Assuming a 1 m length of fiber, transmission losses will be below 10% for a total loss rate $L<0.1v_{\parallel}$. For the uncooled case this becomes $L<100$ s^{-1}, which according to Fig. 9 gives a maximum confined transverse kinetic energy of $E_{kmax}/\epsilon_R\approx900$ for Cs and $E_{kmax}/\epsilon_R\approx40$ for Na, each corresponding to a transverse atomic velocity of about 10 cm s^{-1} and 20 cm s^{-1}, respectively. For the cooled case the inequality becomes $L<0.1$ s^{-1}, which according to Fig. 9 gives a maximum confined transverse kinetic energy of $E_{kmax}/\epsilon_R\approx7$ for Cs and is probably impossible to fulfill with Na. This is because its low speed keeps it in the fiber for a second and the evanescent field is too weak to confine it while keeping the spontaneous emission rate sufficiently low.

The required parameters for the uncooled case are realized by an atomic beam with a divergence angle of ±0.1–0.2 mrad. This is a figure which can be reached by using laser cooling for the transverse directions [25]. Since the fiber can start in one vacuum chamber and end in another, any guided atoms should be readily detectable. With a bent or sufficiently long fiber the ballistic background should be negligible [10]. We have not considered coherent propagation in bent fibers. A heuristic discussion of incoherent propagation in a bent fiber (neglecting the influence of spontaneous emission) is given in Ref. [10]. In a bent fiber the longitudinal and transverse motions are no longer decoupled. Consequently, atoms with a certain longitudinal velocity will be guided along the fiber only if its bending radius is large enough. The minimum bending radius can be readily estimated to be $R_{min}\approx\rho_1(2v_{\parallel}/v_{\perp max})^2$, which gives 1000 m for Cs and 170 m for Na in the uncooled case and 10 cm for cooled Cs.

If guidance occurred only via a single transverse atomic wave function, then atomic coherence could potentially be preserved. In practice this is likely to be difficult to achieve. The situation is analogous to propagation of light in conventional optical fibers. Single-mode propagation maintains coherence, while multimode propagation does not. Naively this is because in the multimode case the light can take different paths through the fiber, with different phase lengths. Atomic coherence is also de-

termined by the atomic energy dispersion. Unlike light, monochromatic sources of atoms are not yet available. Hence achieving coherent propagation with a significant atomic flux will be difficult.

In conclusion we have shown that achievable evanescent fields in hollow optical fibers can be used to guide atoms with realistic transitions. If a suitable atomic source were available this could be done while maintaining the de Broglie wave coherence. Applications to large area atomic interferometry might then be considered.

ACKNOWLEDGMENTS

APPENDIX

In this appendix we give the conditions that have to be fulfilled in order to solve Maxwell's equations for the piecewise constant refractive index profile (1). We have to guarantee the continuity of H and the tangential component of the electric field E_t as well as the normal component of the dielectric displacement vector $\varepsilon_0n^2E_n$. Using (3) we find that this is equivalent to demanding the continuity of h_z, h_ϕ, h_r, e_z, e_ϕ, and n^2e_r. Making use of the relation between the transverse and longitudinal components (4) and the ansatz (5) as well as its magnetic counterpart, we can easily show that it suffices to demand the continuity of h_z, h_ϕ, e_z, and e_ϕ at both boundaries. This leads to the following set of equations.

Continuity of h_z at both boundaries implies

$$c_5I_\nu(U)=c_6J_\nu(X)+c_7Y_\nu(X), \qquad (A1)$$

$$c_8K_\nu(\tilde{W})=c_6\,J_\nu(\tilde{X})+c_7\,Y_\nu(\tilde{X}). \qquad (A2)$$

Continuity of h_ϕ implies

$$c_6J_\nu(X)+c_7p_HY_\nu(X)-c_5p_FI_\nu(U)$$

$$=\frac{ik}{\beta\nu}\sqrt{\frac{\epsilon_0}{\mu_0}}\{n_F^2p_HX[c_2J_\nu'(X)+c_3Y_\nu'(X)]$$

$$-c_1p_FUI_\nu'(U)\}, \qquad (A3)$$

$$c_6p_{Cl}J_\nu(\tilde{X})+c_7p_{Cl}Y_\nu(\tilde{X})-c_8p_FK_\nu(\tilde{W})$$

$$=\frac{ik\rho_2}{\beta\nu\rho_1}\sqrt{\frac{\epsilon_0}{\mu_0}}\{n_F^2p_{Cl}X[c_2J_\nu'(\tilde{X})+c_3Y_\nu'(\tilde{X})]$$

$$-c_4n_C^2p_FWK_\nu'(\tilde{W})\}. \qquad (A4)$$

Continuity of e_z implies

$$c_1 I_\nu(U) = c_2 J_\nu(X) + c_3 Y_\nu(X), \qquad (A5)$$

$$c_4 K_\nu(\tilde{W}) = c_2 J_\nu(\tilde{X}) + c_3 Y_\nu(\tilde{X}). \qquad (A6)$$

Continuity of e_ϕ implies

$$c_2 p_H J_\nu(X) + c_3 p_H Y_\nu(X) - c_1 p_F I_\nu(U)$$

$$= \frac{ik}{\beta\nu}\sqrt{\frac{\mu_0}{\epsilon_0}}\{c_5 p_F U I_\nu'(U)$$

$$- p_H X[c_6 J_\nu'(X) + c_7 Y_\nu'(X)]\}, \quad (A7)$$

$$c_2 p_{\mathrm{Cl}} J_\nu(\tilde{X}) + c_3 p_{\mathrm{Cl}} Y_\nu(\tilde{X}) - c_4 p_F K_\nu(\tilde{W})$$

$$= \frac{ik\rho_2}{\beta\nu\rho_1}\sqrt{\frac{\mu_0}{\epsilon_0}}\{c_8 p_F W K_\nu'(\tilde{W})$$

$$- p_{\mathrm{Cl}} X[c_6 J_\nu'(\tilde{X}) + c_7 Y_\nu'(\tilde{X})]\}. \quad (A8)$$

Here we used the abbreviations $p_H = k^2 - \beta^2$ and $p_{F,\mathrm{Cl}} = n_{F,\mathrm{Cl}}^2 k^2 - \beta^2$. The tilde in some of the equations indicates that the argument of the various Bessel functions has to be taken at the core-cladding interface, e.g., $\tilde{X} = X\rho_2/\rho_1$.

[1] J.P. Gordon and A. Ashkin, Phys. Rev. A **21**, 1606 (1980).

[2] R.J. Cook and R.K. Hill, Opt. Commun. **43**, 258 (1982).

[3] R. Deutschmann, W. Ertmer, and H. Wallis, Phys. Rev. A **47**, 2169 (1993).

[4] H. Wallis, J. Dalibard, and C. Cohen-Tannoudji, Appl. Phys. B **54**, 407 (1992).

[5] M.A. Kasevich, D.S. Weiss, and S. Chu, Opt. Lett. **15**, 607 (1990).

[6] V.I. Balykin, V.S. Letokhov, Yu.B. Ovchinnikov, and A.I. Sidorov, Phys. Rev. Lett. **60**, 2137 (1988).

[7] J.V. Hajnal, K.G.H. Baldwin, P.T.H. Fisk, H.-A. Bachor, and G.I. Opat, Opt. Commun. **73**, 331 (1989).

[8] R. Deutschmann et al. (unpublished).

[9] C.G. Aminoff, A.M. Steane, P. Bouyer, P. Desbiolles, J. Dalibard, and C. Cohen-Tannoudji, Phys. Rev. Lett. **71**, 3083 (1993).

[10] C.M. Savage, S. Marksteiner, and P. Zoller, in *Fundamentals of Quantum Optics III*, edited by F. Ehlotzky (Springer-Verlag, Berlin, 1993).

[11] The restriction to a WKB approximation is purely technical and is made in order to derive *analytical* estimates for the loss rates. However, the results of this paper, especially Sec. V, are not limited to this approximation. A limitation exists only in the sense that the energetically *highest* guided atomic eigenmode must be well approximated by a WKB wave function.

[12] M.A. Ol'Shanii, Yu. B. Ovchinnikov, and V.S. Letokov, Opt. Commun. **98**, 77 (1993).

[13] A.W. Snyder and J.D. Love, *Optical Waveguide Theory* (Chapman and Hall, London, 1983).

[14] The HE$_{11}$ mode always exists for the standard optical fiber (without a hole). This is not true for the hollow fiber. Below a certain critical core thickness [determined by the cutoff condition $\tan(X) = U/X$ for the asymmetric slab waveguide], we find that the HE$_{11}$ mode exists only for hole radii less than a critical value. For larger hole radii, even this mode is cut off and the fiber becomes opaque ("no-modes" regime in Fig. 2).

[15] The advantage of this configuration is that it is reasonably far away from the no-mode regime. The disadvantage is that it is very close to the multimode region. Even though the fiber is single mode, there exist additional modes with very small attenuation constants.

[16] S. Sudo, I. Yokohama, H. Yasaki, Y. Sakai, and T. Ikegami, IEEE Photon. Technol. Lett. **2**, 128 (1990).

[17] B.R. Mollow, Phys. Rev. A **12**, 1919 (1975).

[18] A.P. Kazantsev, G.I. Surdutovich, and V.P. Yakovlev, *Mechanical Action of Light on Atoms* (World Scientific, Singapore, 1990).

[19] H. B. Casimir and D. Polder, Phys. Rev. **73**, 360 (1948).

[20] M.V. Berry and K.E. Mount, Rep. Prog. Phys. **35**, 315 (1972).

[21] E. Merzbacher, *Quantum Mechanics* (Wiley, New York, 1970).

[22] C.I. Sukenik, M.G. Boshier, D. Cho, V. Sandoghdar, and E.A. Hinds, Phys. Rev. Lett. **70**, 560 (1993).

[23] G. Barton, Proc. R. Soc. London Ser. A **410**, 141 (1987); **410**, 175 (1987).

[24] I.E. Dzyaloshinskii, E.M. Lifshitz, and L.P. Pitaevskii, Adv. Phys. **10**, 165 (1961), Sec. 4.4.

[25] See, e.g., courses by C. Cohen-Tannoudji and W.D. Phillips, in *Fundamental Systems in Quantum Optics*, edited by J. Dalibard, J.M. Raimond, and J. Zinn-Justin (North-Holland, Amsterdam, 1990).